

Excitonic Linewidth Approaching the Homogeneous Limit in MoS₂-Based van der Waals Heterostructures

F. Cadiz,^{1,*} E. Courtade,¹ C. Robert,¹ G. Wang,¹ Y. Shen,² H. Cai,² T. Taniguchi,³ K. Watanabe,³ H. Carrere,¹ D. Lagarde,¹ M. Manca,¹ T. Amand,¹ P. Renucci,¹ S. Tongay,² X. Marie,¹ and B. Urbaszek^{1,†}

¹Université de Toulouse, INSA-CNRS-UPS, LPCNO, 135 Avenue de Rangueil, 31077 Toulouse, France

²School for Engineering of Matter, Transport and Energy, Arizona State University, Tempe, Arizona 85287, USA

³National Institute for Materials Science, Tsukuba, Ibaraki 305-0044, Japan

(Received 1 February 2017; revised manuscript received 15 March 2017; published 18 May 2017)

The strong light-matter interaction and the valley selective optical selection rules make monolayer (ML) MoS₂ an exciting 2D material for fundamental physics and optoelectronics applications. But, so far, optical transition linewidths even at low temperature are typically as large as a few tens of meV and contain homogeneous and inhomogeneous contributions. This prevented in-depth studies, in contrast to the better-characterized ML materials MoSe₂ and WSe₂. In this work, we show that encapsulation of ML MoS₂ in hexagonal boron nitride can efficiently suppress the inhomogeneous contribution to the exciton linewidth, as we measure in photoluminescence and reflectivity a FWHM down to 2 meV at $T = 4$ K. Narrow optical transition linewidths are also observed in encapsulated WS₂, WSe₂, and MoSe₂ MLs. This indicates that surface protection and substrate flatness are key ingredients for obtaining stable, high-quality samples. Among the new possibilities offered by the well-defined optical transitions, we measure the homogeneous broadening induced by the interaction with phonons in temperature-dependent experiments. We uncover new information on spin and valley physics and present the rotation of valley coherence in applied magnetic fields perpendicular to the ML.

DOI: 10.1103/PhysRevX.7.021026

Subject Areas: Condensed Matter Physics,
Materials Science, Spintronics

I. INTRODUCTION

The first member of the transition metal dichalcogenides (TMDC) to be established as a direct gap semiconductor in monolayer (ML) form was MoS₂ [1,2], which has resulted in a global research effort exploring this promising 2D semiconductor family [3–16]. First prototype device applications, such as transistors [17–19] and light emitters [20–22], have shown the promise of this atomically thin material for electronics and optoelectronics. Another motivation for research into MoS₂ is the high natural abundance of the naturally occurring mineral molybdenite [23]. Because of their apparent superior optical quality as compared to ML MoS₂, recent research on layered TMDC materials with an emphasis on challenging experiments in valleytronics and light-matter interaction has focused mainly on the closely related monolayer materials WSe₂, WS₂, and MoSe₂ [6,24]. In the transition metal

diselenide MLs, the FWHM of the neutral exciton transition at the optical band gap is typically of the order of 10 meV (50 meV) at $T = 4$ K (300 K) when exfoliated onto Si/SiO₂ substrates [25–27].

Here, we show that the optical transition linewidth in MoS₂ MLs encapsulated in hexagonal boron nitride (hBN) [28] reaches values down to 2 meV at $T = 4$ K; see for example Figs. 3(a) and 4(d). This is a major improvement on the usually reported emission linewidth of \approx 50 meV at low temperature [9,14,16,29–34]. The high-quality van der Waals heterostructures [35] we investigate here allow us to access new information on their optical and spin-valley properties.

- (1) The FWHM of the transition linewidth measured in photoluminescence (PL) and reflectivity down to 2 meV provides a new upper limit for the homogeneous linewidth of the exciton transition, corresponding to a lower limit for exciton radiative lifetime of $T_1 \sim 330$ fs. The linewidth of 2 meV is even smaller than a previously reported value of the homogeneous linewidth in ML MoS₂ on SiO₂ substrates (4.5 meV) measured with four-wave mixing [36]. In temperature-dependent experiments we measure the broadening of the optical transition linewidth due to interactions with acoustic and optical phonons. The proximity of the Γ point close

*cadiz@insa-toulouse.fr

†urbaszek@insa-toulouse.fr

in energy to the valence band maximum at the K point in MoS₂ [37–39] might be at the origin of the strong broadening observed when approaching room temperature.

- (2) Remarkably, the emission linewidth and intensity in our hBN/ML MoS₂/hBN structures are unchanged following several cool-down cycles to $T = 4$ K and exposure to laser radiation. This is in contrast to the variable optical response of uncapped MoS₂ [40] and WS₂ [41,42] MLs exfoliated onto Si/SiO₂ substrates, which often depends also on cool-down procedure and sample history. Reproducibility and stability are essential to better understand the unusual optical properties of these materials [6,24] and to prepare possible device applications. We observe these narrow transition lines in different ML MoS₂ samples exfoliated from different bulk material (i) grown by chemical vapor transport (CVT) (see Sec. V) and (ii) commercially available crystals. We also show that narrow linewidths can be achieved in other TMDC MLs via hBN encapsulation
- (3) The narrow linewidth allows us to distinguish spectrally the emission from the nonidentical valleys K^+ and K^- in MoS₂ as they are split by the valley Zeeman effect [43–48]. We are able to determine the longitudinal exciton Landé g factor in magnetic fields below 10 T in a commercial magnetocryostat. Because of the large linewidth of uncapped samples, this measurement has so far only been possible in pulsed field facilities generating several tens of tesla [33,34]. We find for the neutral exciton $g_X = -1.7 \pm 0.1$, different from earlier reports on unprotected samples that suggested $g_X = -4$. Here, we discuss the possible impact of doping (i.e., contributions from charged excitons) and the dielectric environment. We also show the *generation* and *rotation* of robust valley coherence, a coherent superposition of valley states using the chiral optical selection rules [26], an important step towards full optical control of valley states in these 2D materials [49–51].

II. NEUTRAL EXCITON TRANSITION IN PL AND REFLECTIVITY

A. Sharp linewidth in hBN/ML TMDC/hBN

Figure 1(a) shows an optical micrograph and the corresponding schematic of a van der Waals heterostructure in which a MoS₂ ML is encapsulated in hBN. The photoluminescence spectrum at low temperature of these encapsulated MoS₂ MLs exhibits a very narrow neutral exciton emission (X^0) at energies between 1.93–1.95 eV with a linewidth (FWHM) varying between 2 and 5 meV depending on the sample used and the detection spot position, where the detection spot diameter is $\approx 1 \mu\text{m}$ (see Sec. V). The low-temperature linewidth in our capped samples is more than 1 order of magnitude smaller than the one observed for the usual broad peak reported in most studies

for MoS₂ [9,14,16,29–34]. This transition usually attributed to the neutral exciton is possibly merged with a broad charged exciton and/or defect contribution, as discussed recently [40]. The PL and reflectivity FWHM measured here is for certain samples smaller than the homogeneous linewidth extracted by means of four-wave mixing techniques for MLs on SiO₂ [36]. This represents a major breakthrough since MoS₂ is the most abundant TMDC found in nature. For comparison, PL and reflectivity give neutral exciton linewidth down to 4 meV in hBN encapsulated WSe₂ MLs [52–55], a material which so far has been considered to have superior optical compared to MoS₂.

A typical PL emission spectrum of a capped sample is shown in Fig. 1(b) (filled curve) under a $50\text{-}\mu\text{W}$ cw laser excitation at 2.33 eV. The neutral exciton emission, identified by polarization-resolved experiments (shown in Sec. III), corresponds to the main feature observed in the differential reflectivity spectrum in the same figure.

Note that almost no signature of charged excitons or defect-related emission is observed in these MLs. In contrast, the typical spectrum of a MoS₂ ML deposited directly onto the SiO₂ substrate (black curve) exhibits a very large and broad defect-related emission followed by charged exciton (trion) emission (FWHM 38 meV) and a neutral exciton emission (FWHM 16 meV) [56] whose intensity drops dramatically after a few minutes of laser exposure due to laser-induced doping of these MLs [40] (here, the spectrum was recorded within the first 0.5 sec following laser exposure). The intensity stemming from the neutral exciton in our hBN-protected samples is at least 1 order of magnitude higher than in unprotected ones; for a fully quantitative comparison cavity effects need to be taken into account [57].

Important for reproducibility, no evolution or hysteresis of the PL spectrum is observed even after several minutes of exposure to $\sim 500\text{-}\mu\text{W}$ excitation and after several temperature cycles $4 \leftrightarrow 300$ K. We also observe a significant narrowing of the neutral exciton emission in other TMDC monolayers when they are encapsulated with hBN, as shown in Fig. 2. The typical spectra obtained when MLs are deposited directly onto SiO₂ are shown for comparison. In Table I, the measured PL linewidths at room and cryogenic temperatures for the encapsulated MLs are summarized.

These results demonstrate that capping the MLs with hBN allows us to address the intrinsic high optical quality of these 2D crystals, and protects them from possible charge transfers and local electric field fluctuations coming from the substrate. The layer of hBN below the TMDC acts as a spacer so that the surface roughness of SiO₂ is not transferred to the ML [58,59]. This also suggests that for certain applications no acid treatment of the surface is needed if the freshly exfoliated sample is capped immediately with hBN [60]. Note that at low temperatures, the neutral exciton X^0 line is redshifted by 20–30 meV in

capped samples with respect to unprotected ones. This was also observed previously in capped WSe₂ MLs [52–54], and may be due to a different dielectric environment when the ML is capped with hBN [61,62] or to a different strain when the MLs are not directly in contact with the SiO₂ substrate. In recent studies addressing this problem in ML WSe₂, it has been suggested that this small redshift of the emission is the result of two substantial shifts compensating each other [62]: the neutral exciton emission energy, also called the optical bandgap, is given by the difference between the free carrier bandgap E_g and the exciton binding energy E_B . Encapsulation in hBN results in a smaller exciton binding energy but also in a lower free carrier bandgap. Although both energies might have changed considerably, as we measure their difference, we only observe a very small shift compared to the optical bandgap of non-encapsulated samples.

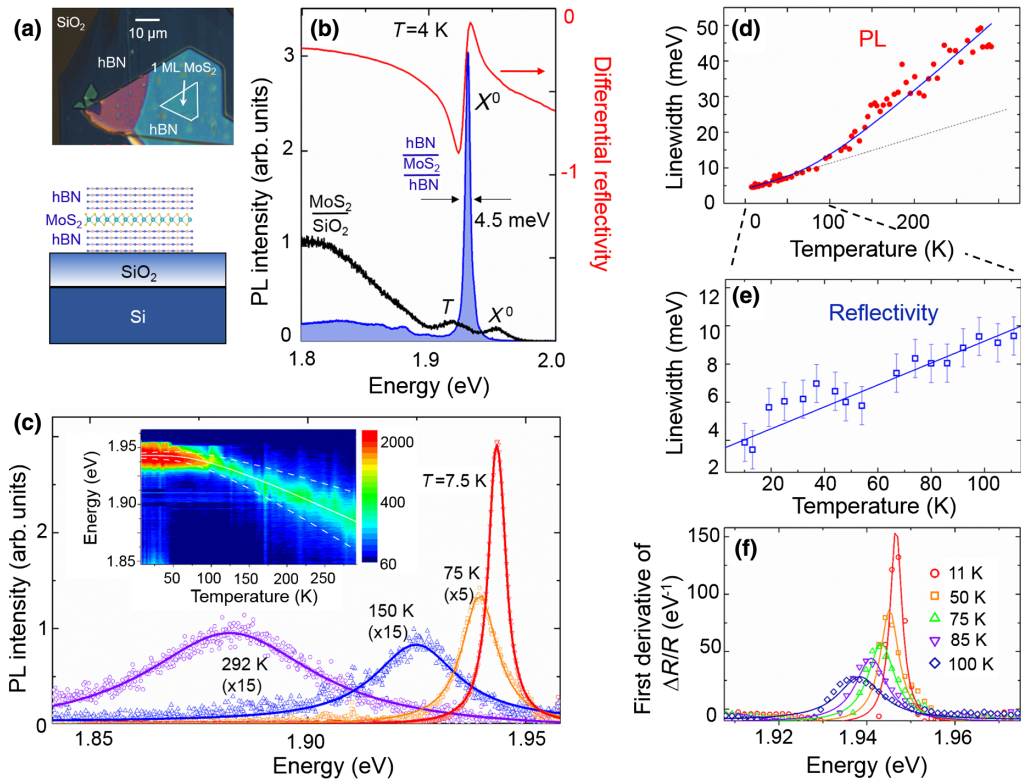


FIG. 1. (a) Top: Optical microscope image of van der Waals heterostructure hBN/ML MoS₂/hBN. Bottom: Schematic of sample (b) PL spectrum (filled curve) at $T = 4$ K for one capped ML when excited with a 2.33-eV cw laser with a power density of $50 \mu\text{W}/\mu\text{m}^2$. The neutral exciton transition, which is also the main feature of the differential reflectivity spectrum (red curve), exhibits a very narrow linewidth of 4.5 meV for this particular sample. Also shown is the PL spectrum of an uncapped MoS₂ ML deposited directly onto the SiO₂ substrate (black curve) measured under the same conditions. (c) PL spectrum of a capped sample for selected sample temperatures. The inset shows a color map revealing the temperature evolution of the spectrum's intensity. The white full line tracks the evolution of the peak position according to Eq. (1), whereas the dashed lines are a guide to the eye indicating the linewidth (FWHM). The excitation density is kept as low as $1 \mu\text{W}/\mu\text{m}^2$. (d) Temperature evolution of the neutral exciton linewidth extracted from the PL spectra when excited with $1 \mu\text{W}/\mu\text{m}^2$. Typical error bars are ± 1 meV (± 5 meV) at 4 K (300 K). The solid line is a fit according to Eq. (2), and the dashed line represents the linear term which dominates at low temperatures. (e) Linewidth extracted from the first derivative of the differential reflectivity as a function of temperature. The linear fit is consistent with a broadening induced by scattering with low-energy acoustic phonons. (f) The first derivative of the differential reflectivity for selected temperatures, centered around the X^0 absorption.

B. Temperature-induced line broadening

Figure 1(c) shows the PL spectrum of an encapsulated MoS₂ sample for selected temperatures, revealing a blueshift of 62 meV and a narrowing by a factor of 10 for the neutral exciton emission when cooling down the sample from 300 to 4 K. The inset is a color map showing the evolution of the PL intensity as a function of temperature for a fixed low laser power of $1 \mu\text{W}$ at 1.96 eV. When going from room temperature to 4 K, the intensity increases significantly and the linewidth narrows down to only a few meV. In addition to the reduction of nonradiative recombination on defects, the overall, not monotonous increase in intensity when reaching low temperature may be due to a competition between bright and dark excitonic states and possibly indicates that ML MoS₂ belongs to the bright family as ML MoSe₂. Several theoretical calculations have

predicted that the lowest excitonic transition in MoS₂ MLs should be bright [63,64], but this is still debated since the opposite configuration has also been predicted [65]. Here, charge tunable samples [66] or experiments in transverse magnetic fields [67,68] are expected to give a better indication on the dark-bright order in future experiments on these narrow linewidth samples.

The temperature dependence of the PL peak position follows a standard hyperbolic cotangent relation [69]:

$$E_G(T) = E_G(0) - S\langle\hbar w\rangle \{\coth[\langle\hbar w\rangle/(2k_B T)] - 1\}, \quad (1)$$

where $E_G(0)$ is the optical band gap at zero temperature, S is a dimensionless coupling constant, k_B is Boltzmann's constant, and $\langle\hbar w\rangle$ is an average phonon energy. The fitted curve [solid line shown in the inset of Fig. 1(c)] yields $E_G(0) = 1.943$ eV, $S = 1.87$, and $\langle\hbar w\rangle = 24.2 \pm 1.5$ meV. The coupling constant and the average phonon energy are similar to those reported previously in the literature for the TMDC ML family [25,34,41,70,71]. The evolution of the

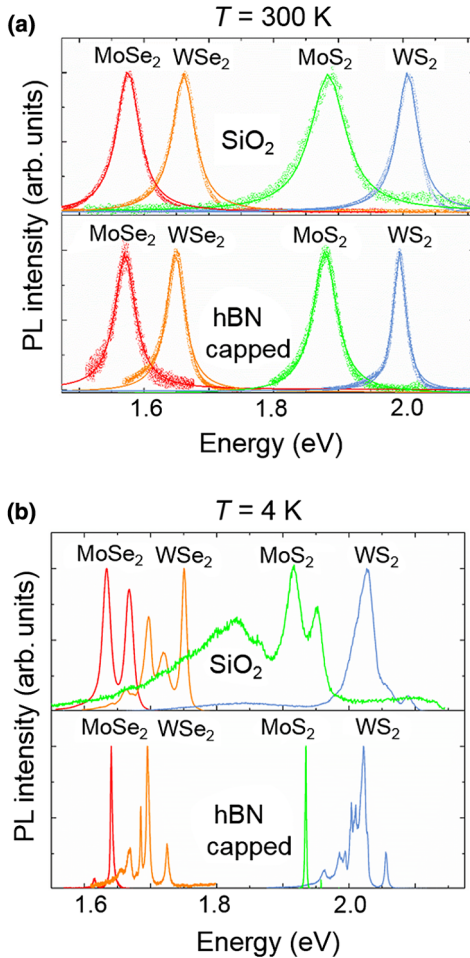


FIG. 2. (a) Typical PL spectra for different TMDC MLs at $T = 300$ K when deposited directly onto SiO₂ (top) and when capped with hBN (bottom). The excitation density is $1 \mu\text{W}/\mu\text{m}^2$. (b) Same as (a) at $T = 4$ K.

linewidth as a function of temperature is shown in Fig. 1(d), and it can be seen that it decreases by more than 1 order of magnitude when passing from room to cryogenic temperatures, which is a signature of an efficient coupling with phonons. The evolution of the linewidth can be phenomenologically approximated by a phonon-induced broadening [36,72]:

$$\gamma = \gamma_0 + c_1 T + \frac{c_2}{e^{\Omega/k_B T} - 1}, \quad (2)$$

where $\gamma_0 = 4 \pm 0.2$ meV and $c_1 = 70 \pm 5 \mu\text{eV/K}^{-1}$ describes the linear increase due to acoustic phonons, and is of the same order of magnitude as the one reported in Refs. [36,73]. The parameter $c_2 = 42.6 \pm 1.2$ meV is a measure of the strength of the phonon coupling and $\Omega = 24.2$ meV is the *averaged* energy of the relevant phonons, which we obtain by fitting the optical band gap energy shift with Eq. (1) for consistency. Note that the value of $c_2 = 42.6$ meV we find here is larger than the 6.5 and 15.6 meV previously reported for WS₂ and MoSe₂ MLs, respectively [72]. Note, however, that the value of c_2 depends strongly on the choice of Ω . In any case, we find that MoS₂ has the broadest PL emission at room temperature, as indicated in Table I. In contrast, WS₂ MLs exhibit the narrowest emission linewidth at room temperature, half the value of MoS₂. So far, no detailed discussion exists on the broadening of MoS₂ MLs since the optical transition linewidth in uncapped samples is too broad. A larger coupling with optical phonons in MoS₂ may be a consequence of the energy proximity between the local maximum of the valence band at Γ and the absolute maxima at the K valleys in MoS₂ MLs [37–39].

In order to exclude any possible problems due to localization effects on the linewidth evolution at low temperatures, we perform reflectivity measurements in addition to PL as a function of temperature in MoS₂ MLs. The first derivative of the differential reflectivity for selected temperatures is shown in Fig. 1(f), and also exhibits a very small linewidth of ~ 3 meV, which broadens roughly linearly as a function of temperature up to 100 K, as shown in Fig. 1(e). A linear fit gives a slope of $61 \pm 5 \mu\text{eV/K}$, similar to the $70 \pm 5 \mu\text{eV/K}$ observed

TABLE I. Neutral exciton linewidth measured on different TMDC monolayers encapsulated with hBN at an excitation density of $1 \mu\text{W}/\mu\text{m}^2$.

Sample	Neutral exciton linewidth (meV)	
	$T = 4$ K	$T = 292$ K
MoS ₂ (Commercial)	2.0–4.5	44–46
MoS ₂ (CPT grown)	3.9–5.0	44–49
MoSe ₂ (VPT grown)	2.4–4.9	34–36
WSe ₂ (Commercial)	3.9–4.2	32–34
WS ₂ (Commercial)	4.3–4.8	23–25

for the PL linewidth. Since reflectivity is sensitive to transitions with a large density of states [74], i.e., free excitons, we conclude from the very similar temperature dependence that the PL also stems dominantly from free neutral excitons. Because of sample inhomogeneity the exciton energy fluctuates by a few meV for different points on the sample. The largest energy difference we measure for the exciton PL energy between two extreme positions on the same flake is 10 meV [75].

III. VALLEY POLARIZATION AND VALLEY COHERENCE MANIPULATION

A. Measurements without applied magnetic fields

The strong excitonic resonances with sharp linewidth in our sample make it possible to study optically the valley polarization in ML MoS₂ in great detail. Here, we benefit from the chiral optical selection rules in TMDC monolayers, which allow optical excitation in the K⁺ or K⁻ valley, using σ⁺ or σ⁻ polarized laser excitation, respectively [26,30,76–78]; see scheme in Fig. 3(a). Detailed studies of valley polarization and coherence have so far mainly focused on ML WSe₂, due to the comparatively narrow linewidth and high polarization degree of the emission [26,79]. Our results below show that the optical quality of ML MoS₂ is high enough to measure the Landé g factor with high accuracy and study valley coherence rotation. In this section, all experiments are carried out at T = 4 K.

Excitation of MoS₂ MLs with a cw, circularly σ⁺ polarized laser results in strongly σ⁺ polarized PL of the neutral exciton X⁰, as shown in Fig. 3(b) [see also the spectra in Fig. 4(a)]. We measure a high circular polarization degree of the PL of P_c ∼ 30% corresponding to initialization of valley polarization. Remarkably, the measured value of P_c is very robust and is independent of the explored laser excitation density, which spans 4 orders of magnitude.

We also explore the generation of robust valley coherence [26] in these capped MLs. As circularly polarized laser excitation induces valley polarization, excitation with a linearly polarized laser can generate a coherent superposition of valley states in the ML, referred to as valley coherence or optical alignment of excitons [80]. As shown in Fig. 3(c), excitation with a linearly polarized laser results in a highly linearly polarized PL emission for the neutral exciton, with a degree of linear polarization as high as P_{lin} ∼ 55% in steady state [the polarization-resolved components of the PL are shown in Fig. 4(d)]. Note that the same excitation energy is used for the measurements shown in Fig. 3(b). Obtaining higher P_{lin} than P_c in experiments is technically possible in 2D exciton systems, where the main exciton spin relaxation mechanism is due to the exchange Coulomb interaction between the electron and hole [81], which can be seen as an effective magnetic field. The

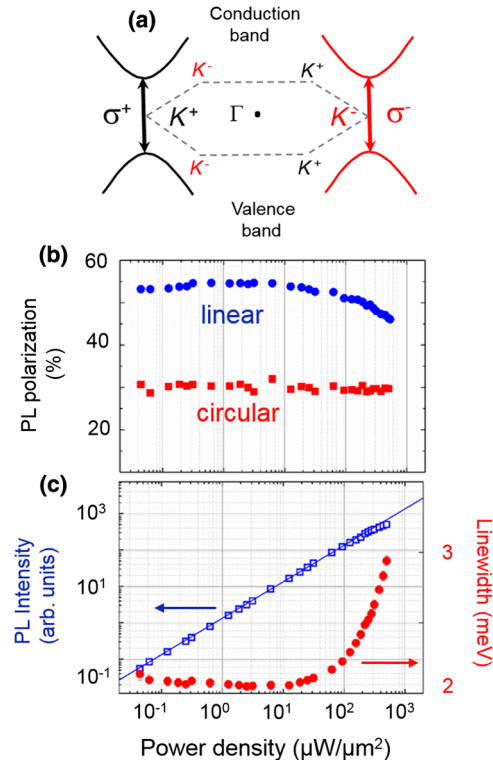


FIG. 3. (a) Chiral optical selection rules for interband optical transitions in nonequivalent valleys K⁺ and K⁻ [30,76]. (b) hBN/ML MoS₂/hBN. Degree of linear PL polarization $P_{\text{lin}} = (I^X - I^Y)/(I^X + I^Y)$ and circular polarization $P_c = (I^{\sigma^+} - I^{\sigma^-})/(I^{\sigma^+} + I^{\sigma^-})$ for linearly and circularly polarized excitation, respectively, as a function of laser power density. Laser energy 1.96 eV, T = 4 K. (c) Integrated PL intensity (open squares) and linewidth (full circles) as a function of excitation power density. The full line represents a linear relationship between intensity and power density. Laser energy 1.96 eV, T = 4 K.

magnitude and direction of this field depend on the exciton center of mass momentum, which changes due to scattering events. The corresponding effective field is seen by the exciton as fluctuating; see Refs. [79,82] for details of this process in TMDC monolayers. In the motional narrowing regime the momentum scattering time is much shorter than the exciton precession time in the exchange field. In this situation the transverse spin relaxation time T_{S2} , which corresponds to the relaxation time of the valley coherence between |+⟩ and |−⟩ exciton states, can be as long as $T_{S2} \approx 2T_{S1}$. Here, T_{S1} is the relaxation time between |+⟩ and |−⟩ exciton states (circular depolarization time). How the exact ratio between P_{lin} and P_c depends on the sample and experimental parameters other than the excitation power we investigate here needs to be studied in future experiments.

Note that the valley coherence starts to drop for excitation densities above 50 μW/μm², probably due to the combined effect of exciton-exciton interactions [83] and

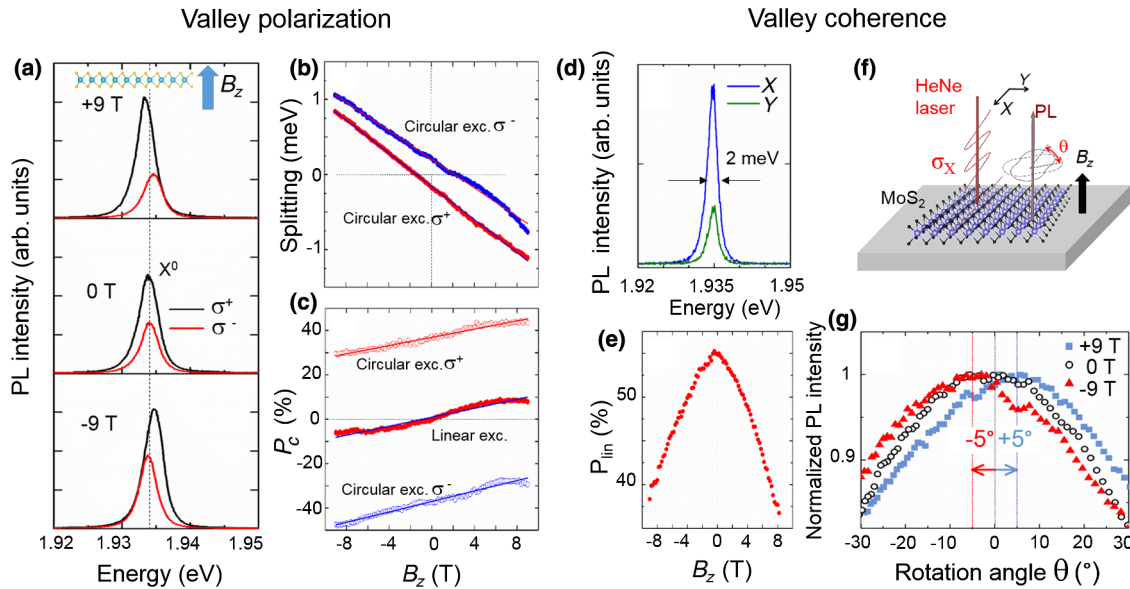


FIG. 4. $T = 4$ K. hBN/ML MoS₂/hBN. (a) The left-hand panel shows typical PL spectra for a capped MoS₂ ML under σ^+ circularly polarized excitation at selected values of the applied magnetic field B_z . Both circularly polarized components of the PL are shown. (b) Zeeman splitting between both circular components of the PL for σ^+ and σ^- polarized excitation at $10 \mu\text{W}/\mu\text{m}^2$. The measured splitting corresponds to an exciton g factor of $g_X = -1.7 \pm 0.1$. (c) Degree of circular polarization P_c as a function of the magnetic field and for different incident polarization of the excitation laser. (d) Linearly polarized components of the PL spectrum after linearly polarized excitation along the X direction at 633 nm. The X^0 emission is highly colinearly polarized, revealing robust valley coherence. (e) Degree of linear polarization P_{lin} following linear excitation as a function of the magnetic field. (f) Schematic of the experimental configuration used to control the valley coherence. (g) PL intensity under linear excitation as a function of the angle of the linear polarization analyzer, for selected values of the magnetic field. A rotation of $\pm 5^\circ$ is observed for the PL polarization at $B_z = \pm 9$ T.

sample heating. The X^0 integrated intensity depends linearly on the excitation density, as shown in Fig. 3(c), and the linewidth increases rapidly for laser powers above $100 \mu\text{W}/\mu\text{m}^2$. This broadening can be a signature of an excitation-induced dephasing that may also be responsible for the observed drop of the valley coherence. Note that the absence of charged exciton emission in PL and in reflectivity suggests that this dephasing is dominated by exciton-exciton interactions, and not by exciton-carrier collisions. Local heating of the sample may also play a role, since at the highest power density used, the X^0 emission redshifts by 0.6 meV, which would correspond, according to Eq. (1), to a local heating up to ~ 30 K.

B. Valley Zeeman splitting and field-induced valley polarization

Measuring the Landé g factor is important for spin-valley physics, as it determines the energy separation achievable between the different polarization states [43–48]. The g factor, closely related to the effective mass tensor, also gives a fingerprint of the impact of different bands on the optical transitions [45,48,84]. In addition, spectacular effects are expected for monolayers with tunable electron density, where the evolution of the valley polarization and the valley Zeeman splitting has been interpreted in terms of a Fermi-polaron model for excitonic transitions; i.e., the

simple definitions of neutral exciton and trion are replaced by the attractive and repulsive polaron [10,85,86].

Thanks to the very narrow exciton emission linewidth in our protected samples, we are able to perform magneto-PL experiments and observe a clear valley Zeeman splitting at moderate magnetic fields. As shown in the schematics of Fig. 4(a), a magnetic field up to ± 9 T is applied perpendicularly to the ML plane and the circular components of the PL are recorded as a function of the magnetic field. Figure 4(a) shows the polarization-resolved PL spectra at $T = 4$ K for different values of the magnetic field using a circularly polarized cw laser at 1.96 eV with a $10-\mu\text{W}/\text{cm}^2$ power density. Note that the linewidth is comparable to the typical valley Zeeman splitting Δ_z at 10 T, defined as the shift between the σ^+ and σ^- polarized components of the PL. This energy splitting is found to depend linearly on the applied magnetic field [as shown in Fig. 4(b)], and using $\Delta_z = g_X \mu_B B_z$, where μ_B is the Bohr magneton, we extract an exciton g factor of $g_X = -1.7 \pm 0.1$. Reducing the incident power by 4 orders of magnitude did not result in any measurable change in the extracted g factor.

In addition, we note that the circular polarization of the PL can be varied with the magnetic field, as shown in Fig. 4(c). At high positive magnetic fields, the valley splitting shifts the K^+ valley to lower energies, favoring the population of this valley in steady-state conditions. In contrast, at high negative magnetic fields, populating the

K^+ valley is energetically unfavorable, and as a consequence, there is a reduction of the steady-state valley polarization. Independent of the incident polarization of the laser, we observe an increase of the valley polarization at a rate of $1\% / T$. In addition to the arguments presented on polarization changes due to transfer of population between the bright states also other mechanisms can play a role. For instance, coupling to optically dark states can also vary as a function of the applied magnetic field and could change the emission intensities measured in the circular polarization basis.

In the literature, only a few reported experimental values exist for the exciton g factor on MoS_2 MLs [33,34] between $g_X = -4$ and $g_X = -4.5$, obtained with magnetoreflectivity measurements on CVD-grown MoS_2 MLs. In order to rule out any possible modification of the g factor induced by the hBN encapsulation, we perform magneto-PL on uncapped MoS_2 MLs deposited directly onto SiO_2 substrates. In order to be able to identify the neutral exciton transition, the sample is first treated with bis(trifluoromethane)sulfonimide (TFSI) [56,60], so that the emission coming from defects is strongly reduced. In order to minimize the impact of laser-induced doping of the ML and to avoid a complete disappearance of the X^0 feature in the PL spectra, a maximum laser power of $30 \mu\text{W}$ is used [40]. Typical spectra are shown in Fig. 5(a), dominated by a trion peak of 32-meV linewidth and a smaller neutral exciton peak of 16-meV linewidth. The extracted Zeeman splitting for the neutral exciton, shown in Fig. 5(b), is consistent with a g factor of $g_X = -1.95 \pm 0.2$, close to the value obtained in capped MLs (Fig. 4). For the trion, we find a larger g factor of $g_T = -6.6 \pm 0.2$. Note that we cannot exclude a contribution of defect-related emission to the measured g factor of the trion peak due to its larger linewidth. Our measurements suggest that the neutral exciton g factor of MoS_2 MLs might be intrinsically smaller (in magnitude) than for diselenide MLs and is different from the commonly observed value

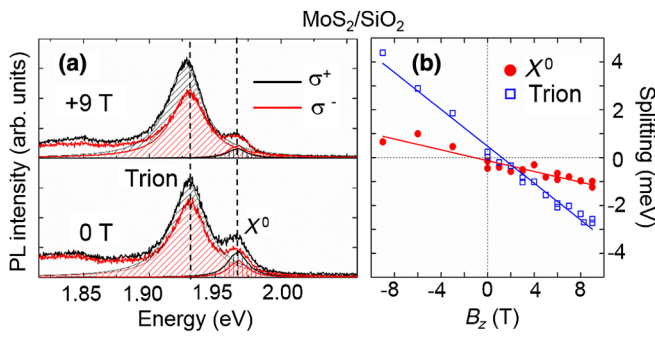


FIG. 5. $T = 4$ K. ML $\text{MoS}_2/\text{SiO}_2/\text{Si}$. (a) Typical PL spectra for an acid-treated, uncapped MoS_2 ML at selected values of the applied magnetic field. A multiple-Lorentzian fit is employed in order to extract the Zeeman splitting of both neutral and charged exciton (trion) lines, shown in (b). Valley Zeeman splitting as a function of the applied field B_z . Landé g factors of $g_X = -1.9 \pm 0.2$ and $g_T = -6.6 \pm 0.2$ are found.

$g_X \approx -4$ [43–45,47,48]. Variations in the measured neutral exciton g factor can have different reasons: (i) different strain in CVD-grown MLs as compared to encapsulated monolayers may play a role, (ii) comparing g factors in samples of different origin with different electron concentrations is difficult due to the possible impact of many-body interactions [10,85,86], (iii) eventually, in unprotected samples with considerably broader linewidth, magnetoreflectivity may provide a g factor that is an average of exciton and trion g factors.

C. Rotation of valley coherence

In addition to the optical generation of valley polarization, the optical generation of valley coherence has also thus far been mainly studied in WSe_2 and WS_2 and not MoS_2 due to the broad transition linewidth. Generation of valley coherence is achieved optically by linearly polarized excitation σ_X , which results in strongly linearly polarized neutral exciton (X^0) emission [26]. Recent experiments have shown that this valley polarization can be rotated in ML WSe_2 and WS_2 [49–51], a first important step towards full control of valley states [87]. The MoS_2 ML is excited by a linearly polarized (σ_X) continuous wave He-Ne laser (1.96 eV) to generate valley coherence (i.e., optical alignment of excitons [80]). Our target is to detect the neutral exciton X^0 valley coherence in the linear basis in PL emission. A liquid-crystal-based linear polarization rotator is applied in the detection path, to detect a possible rotation of the linear basis of the PL signal with respect to the initial linear excitation basis given by the laser. The rotation angle θ can be tuned by varying B_z . This approach avoids any macroscopic mechanical movement during the measurement and gives an accurate map of the angle-dependent PL intensity, as schematically illustrated in Fig. 4(f); the full data set is plotted in Fig. 4(g). The initial linear polarization corresponds to $\theta = 0^\circ$ and we rotate the linear polarizer in detection and record for which angle θ the PL emission is maximized.

In this experiment the external magnetic field lifts the valley degeneracy [43–48] and results in a change of the oscillation frequency of the coherent superposition of valley states. This corresponds to a rotation of valley coherence (i.e., the exciton pseudospin), and we clearly measure this rotation in our experiments with angles up to $\pm 5^\circ$ at $B = \pm 9$ T. As the rotation is measurable in our simple steady-state experiment, we can conclude that the valley coherence time of the neutral excitons is at least roughly of the order of the PL emission time in our sample.

A different measurement is presented in Fig. 4(e): we show the evolution of the linear polarization following linear excitation as a function of the magnetic field, but keeping the linear basis in detection fixed. A significant decrease is observed, which can have several origins. First, strong rotation of valley coherence resulting in small projection in the initial basis. As we measure only

a small rotation angle θ , this rotation can only be partially responsible for the observed drop of the linear polarization. A second cause for the decrease in the detected linear polarization can be dephasing induced during the PL lifetime [79]. Note that a smaller rotation angle of the PL with respect to the one observed in WSe₂ [50] and WS₂ [49] MLs (characterized by larger g factors) is indeed expected for a smaller exciton g factor measured in our sample.

IV. CONCLUSION AND PERSPECTIVES

In conclusion, we show that encapsulating TMDC MLs in hBN allows us to access the intrinsic high optical quality of these 2D crystals. Key roles of the top and bottom hBN layers are the protection of the sample surface from possible physio- and chemiosorption during the experiment, providing an atomically flat surface for sample exfoliation to avoid ripples [58] and preventing optical doping from the SiO₂. The observed linewidth of a few meV at low temperatures is the smallest ever reported for this material and provides an upper limit for the homogeneous linewidth (≤ 2 meV) and a lower limit for exciton radiative lifetime (≥ 0.33 ps). This confirms that the large PL linewidth of tens of meV reported for uncapped MoS₂ on SiO₂ is mainly caused by inhomogeneous broadening [36]. No hysteresis of the PL after laser exposure or temperature cycles is observed. Also, no clear signature of charged excitons and/or trapped excitons is visible in these protected flakes obtained from bulk material of different origins. The temperature-induced broadening of the X^0 transition in PL and in reflectivity follows the same linear relationship up to 100 K, indicating that the PL linewidth contains only small inhomogeneous contributions.

We also revisit magneto-PL measurements with these high-quality samples and measure a neutral exciton Landé factor of $g_X = -1.7 \pm 0.1$ in MoS₂ that is smaller in magnitude than the typical value -4 reported for other members of the TMDC family and for CVD-grown MoS₂ MLs on SiO₂ [43–45,47,48]. Excitation of this high-quality ML with a linearly polarized, nonresonant laser creates a robust coherent superposition of valley states and a high steady-state linear polarization of the PL (55%). We show rotation of this coherent superposition of valley states in applied magnetic fields up to 9 T.

The well-defined optical transitions and negligible defect emission will allow us in the future to further explore these stable MoS₂ samples; for example, the exciton resonance can be tuned in resonance with optical cavity modes to explore strong coupling between light and matter in microcavities [7,8] with the added possibility of valley-specific optical excitations [88,89]. Also, all time-resolved experiments using pulsed laser, such as pump-probe spectroscopy, time-resolved PL, and four-wave mixing [12,31,36,90,91], will benefit from these samples with much higher threshold for optical damage as compared to uncapped samples.

ACKNOWLEDGMENTS

We thank ERC Grant No. 306719, ITN Spin-NANO Marie Skłodowska-Curie Grant Agreement No. 676108, ANR MoS2ValleyControl, Programme Investissements d’Avenir ANR-11-IDEX-0002-02, reference ANR-10-LABX-0037-NEXT for financial support. X. M. also acknowledges the Institut Universitaire de France. S. T acknowledges funding from National Science Foundation (DMR-1552220) and CMMI-1561839. K. W. and T. T. acknowledge support from the Elemental Strategy Initiative conducted by the MEXT, Japan, and JSPS KAKENHI Grants No. JP26248061, No. JP15K21722, and No. JP25106006.

Note added in proof.—Narrow linewidth emission in hBN encapsulated samples is also reported in [92].

APPENDIX: EXPERIMENTAL DETAILS

1. Optical spectroscopy

The experiments are carried out at variable temperatures $T = 4\text{--}300$ K and in magnetic fields up to ± 9 T in Faraday configuration in a confocal microscope built in a vibration-free, closed cycle cryostat from Attocube. The excitation or detection spot diameter is $\approx 1\text{ }\mu\text{m}$, i.e., smaller than the typical ML diameter. The MoS₂ ML is excited by a continuous wave He-Ne laser (1.96 eV) or at 2.33 eV. The PL signal is dispersed in a spectrometer and detected with a Si-CCD camera. The white light source for reflectivity is a halogen lamp with a stabilized power supply. Faraday effects of the optical setup in applied fields have been systematically calibrated for plotting the valley coherence rotation angle.

2. Samples

In addition to bulk material obtained from 2D semiconductors, Ultrahigh purity MoS₂ crystals are synthesized using a chemical vapor transport technique. Precursor MoS₂ polycrystalline powder is first synthesized by heating and forming a mixture containing stoichiometric amounts of 6N (99.9999% purity) sulfur and molybdenum powders (puratronic quality from Alfa Aesar, Inc. and American Elements, Inc.) at 1020 °C for 14 days in an evacuated sealed quartz ampule at pressures less than 10^{-7} Torr. In a typical polycrystalline MoS₂ powder synthesis, special care is given to attaining high purity by using chemically cleaned and annealed quartz tubes (to prevent degassing), and the mixture is heated from room temperature to 1020 °C in 24 h (to prevent explosion). Approximately 6 g of MoS₂ polycrystals are released together with molybdenum containing a high-purity (6N) MoCl₅ transport agent (at $\sim 4\text{ mg/cm}^3$) in a quartz tube (15.5 mm in diameter and ~ 18 cm in length). Here, MoCl₅ sublimates at low temperature and supplies high Mo-based partial pressure to enhance crystal growth. Successful growth is attained when the source and growth zones are kept at 1065 °C and 1015 °C, respectively, for 12 days.

The growth of MoSe₂ MLs by vapor phase transport technique is described in Ref. [40].

As shown schematically in the inset of Fig. 1(a), we fabricate van der Waals heterostructures by mechanical exfoliation of bulk MoS₂ (CVT grown or commercially available) and hBN crystals [28]. A first layer of hBN is mechanically exfoliated onto a freshly cleaved SiO₂ (90 nm)/Si substrate [93]. The deposition of the subsequent MoS₂ ML and the second hBN capping layer is obtained by repeating this procedure. After the deposition of each individual layer, the sample is annealed at 150 °C during 10 min.

- [1] A. Splendiani, L. Sun, Y. Zhang, T. Li, J. Kim, C.-Y. Chim, G. Galli, and F. Wang, *Emerging Photoluminescence in Monolayer MoS₂*, *Nano Lett.* **10**, 1271 (2010).
- [2] K. F. Mak, C. Lee, J. Hone, J. Shan, and T. F. Heinz, *Atomically Thin MoS₂: A New Direct-Gap Semiconductor*, *Phys. Rev. Lett.* **105**, 136805 (2010).
- [3] J. Kim, X. Hong, C. Jin, S.-F. Shi, C.-Y. S. Chang, M.-H. Chiu, L.-J. Li, and F. Wang, *Ultrafast Generation of Pseudo-Magnetic Field for Valley Excitons in WSe₂ Monolayers*, *Science* **346**, 1205 (2014).
- [4] A. Pospischil, M. M. Furchi, and T. Mueller, *Solar-Energy Conversion and Light Emission in an Atomic Monolayer p-n Diode*, *Nat. Nanotechnol.* **9**, 257 (2014).
- [5] A. Castellanos-Gomez, *Why All the Fuss about 2D Semiconductors?*, *Nat. Photonics* **10**, 202 (2016).
- [6] K. F. Mak and J. Shan, *Photonics and Optoelectronics of 2D Semiconductor Transition Metal Dichalcogenides*, *Nat. Photonics* **10**, 216 (2016).
- [7] S. Dufferwiel *et al.*, *Exciton-Polaritons in van der Waals Heterostructures Embedded in Tunable Microcavities*, *Nat. Commun.* **6**, 8579 (2015).
- [8] X. Liu, T. Galfsky, Z. Sun, F. Xia, E.-c. Lin, Y.-H. Lee, S. Kéna-Cohen, and V. M. Menon, *Strong Light-Matter Coupling in Two-Dimensional Atomic Crystals*, *Nat. Photonics* **9**, 30 (2015).
- [9] T. Korn, S. Heydrich, M. Hirmer, J. Schmutzler, and C. Schüller, *Low-Temperature Photocarrier Dynamics in Monolayer MoS₂*, *Appl. Phys. Lett.* **99**, 102109 (2011).
- [10] M. Sidler, P. Back, O. Cotlet, A. Srivastava, T. Fink, M. Kroner, E. Demler, and A. Imamoglu, *Fermi Polaron-Polaritons in Charge-Tunable Atomically Thin Semiconductors*, *Nat. Phys.* **13**, 255 (2017).
- [11] C. Pöllmann, P. Steinleitner, U. Leierseder, P. Nagler, G. Plechinger, M. Porer, R. Bratschitsch, C. Schüller, T. Korn, and R. Huber, *Resonant Internal Quantum Transitions and Femtosecond Radiative Decay of Excitons in Monolayer WSe₂*, *Nat. Mater.* **14**, 889 (2015).
- [12] T. Jakubczyk, V. Delmonte, M. Koperski, K. Nogajewski, C. Faugeras, W. Langbein, M. Potemski, and J. Kasprzak, *Radiatively Limited Dephasing and Exciton Dynamics in MoSe₂ Monolayers Revealed with Four-Wave Mixing Microscopy*, *Nano Lett.* **16**, 5333 (2016).
- [13] A. Chernikov, C. Ruppert, H. M. Hill, A. F. Rigos, and T. F. Heinz, *Population Inversion and Giant Bandgap Renormalization in Atomically Thin WS₂ Layers*, *Nat. Photonics* **9**, 466 (2015).
- [14] H. Zeng, J. Dai, W. Yao, D. Xiao, and X. Cui, *Valley Polarization in MoS₂ Monolayers by Optical Pumping*, *Nat. Nanotechnol.* **7**, 490 (2012).
- [15] Y. Yu, Y. Yu, C. Xu, A. Barrette, K. Gundogdu, and L. Cao, *Fundamental Limits of Exciton-Exciton Annihilation for Light Emission in Transition Metal Dichalcogenide Monolayers*, *Phys. Rev. B* **93**, 201111 (2016).
- [16] A. Neumann, J. Lindlau, L. Colombier, M. Nutz, S. Najmaei, J. Lou, A. D. Mohite, H. Yamaguchi, and A. Hogege, *Opto-Valleytronic Imaging of Atomically Thin Semiconductors*, *Nat. Nanotechnol.* **12**, 329 (2017).
- [17] B. Radisavljevic, A. Radenovic, J. Brivio, V. Giacometti, and A. Kis, *Single-Layer MoS₂ Transistors*, *Nat. Nanotechnol.* **6**, 147 (2011).
- [18] H. Fang, S. Chuang, T. C. Chang, K. Takei, T. Takahashi, and A. Javey, *High-Performance Single Layered WSe₂ p-FETs with Chemically Doped Contacts*, *Nano Lett.* **12**, 3788 (2012).
- [19] H. Dery and Y. Song, *Polarization Analysis of Excitons in Monolayer and Bilayer Transition-Metal Dichalcogenides*, *Phys. Rev. B* **92**, 125431 (2015).
- [20] R. S. Sundaram, M. Engel, A. Lombardo, R. Krupke, A. C. Ferrari, Ph. Avouris, and M. Steiner, *Electroluminescence in Single Layer MoS₂*, *Nano Lett.* **13**, 1416 (2013).
- [21] J. S. Ross, P. Klement, A. M. Jones, N. J. Ghimire, J. Yan, D. G. Mandrus, T. Taniguchi, K. Watanabe, K. Kitamura, W. Yao, D. H Cobden, and X. Xu, *Electrical Tunable Excitonic Light-Emitting Diodes Based on Monolayer WSe₂ p-n Junctions*, *Nat. Nanotechnol.* **9**, 268 (2014).
- [22] X. Zhang, Q. Liu, J.-W. Luo, A. J. Freeman, and A. Zunger, *Hidden Spin Polarization in Inversion-Symmetric Bulk Crystals*, *Nat. Phys.* **10**, 387 (2014).
- [23] R. G. Dickinson and L. Pauling, *The Crystal Structure of Molybdenite*, *J. Am. Chem. Soc.* **45**, 1466 (1923).
- [24] X. Xu, D. Xiao, T. F. Heinz, and W. Yao, *Spin and Pseudospins in Layered Transition Metal Dichalcogenides*, *Nat. Phys.* **10**, 343 (2014).
- [25] J. S. Ross *et al.*, *Electrical Control of Neutral and Charged Excitons in a Monolayer Semiconductor*, *Nat. Commun.* **4**, 1474 (2013).
- [26] A. M. Jones, H. Yu, N. J. Ghimire, S. Wu, G. Aivazian, J. S. Ross, B. Zhao, J. Yan, D. G. Mandrus, D. Xiao, W. Yao, and X. Xu, *Optical Generation of Excitonic Valley Coherence in Monolayer WSe₂*, *Nat. Nanotechnol.* **8**, 634 (2013).
- [27] G. Wang, X. Marie, I. Gerber, T. Amand, D. Lagarde, L. Bouet, M. Vidal, A. Balocchi, and B. Urbaszek, *Giant Enhancement of the Optical Second-Harmonic Emission of WSe₂ Monolayers by Laser Excitation at Exciton Resonances*, *Phys. Rev. Lett.* **114**, 097403 (2015).
- [28] T. Taniguchi and K. Watanabe, *Synthesis of High-Purity Boron Nitride Single Crystals under High Pressure by Using Ba-BN Solvent*, *J. Cryst. Growth* **303**, 525 (2007).
- [29] G. Kioseoglou, A. T. Hanbicki, M. Currie, A. L. Friedman, D. Gunlycke, and B. T. Jonker, *Valley Polarization and*

- [58] M. K. L. Man, S. Deckoff-Jones, A. Winchester, G. Shi, G. Gupta, A. D. Mohite, S. Kar, E. Kioupakis, S. Talapatra, and K. M. Dani, *Protecting the Properties of Monolayer MoS₂ on Silicon Based Substrates with an Atomically Thin Buffer*, *Sci. Rep.* **6**, 20890 (2016).
- [59] C. R. Dean, A. F. Young, I. Meric, C. Lee, L. Wang, S. Sorgenfrei, K. Watanabe, T. Taniguchi, P. Kim, K. L. Shepard, and J. Hone, *Boron Nitride Substrates for High-Quality Graphene Electronics*, *Nat. Nanotechnol.* **5**, 722 (2010).
- [60] M. Amani, D.-H. Lien, D. Kiriya, J. Xiao, A. Azcatl, J. Noh, S. R. Madhvapathy, R. Addou, Santosh KC, M. Dubey, K. Cho, R. M. Wallace, S.-C. Lee, J.-H. He, J. W. Ager, X. Zhang, E. Yablonovitch, and A. Javey, *Near-Unity Photoluminescence Quantum Yield in MoS₂*, *Science* **350**, 1065 (2015).
- [61] A. Chernikov, T. C. Berkelbach, H. M. Hill, A. Rigos, Y. Li, O. B. Aslan, D. R. Reichman, M. S. Hybertsen, and T. F. Heinz, *Exciton Binding Energy and Nonhydrogenic Rydberg Series in Monolayer WS₂*, *Phys. Rev. Lett.* **113**, 076802 (2014).
- [62] A. Stier, N. P. Wilson, G. Clark, X. Xu, and S. A. Crooker, *Probing the Influence of Dielectric Environment on Excitons in Monolayer WSe₂: Insight from High Magnetic Fields*, *Nano Lett.* **16**, 7054 (2016).
- [63] A. Kormanyos, G. Burkard, M. Gmitra, J. Fabian, V. Zolyomi, N. D. Drummond, and V. Fal'ko, *k · p Theory for Two-Dimensional Transition Metal Dichalcogenide Semiconductors*, *2D Mater.* **2**, 022001 (2015).
- [64] J. P. Echeverry, B. Urbaszek, T. Amand, X. Marie, and I. C. Gerber, *Splitting between Bright and Dark Excitons in Transition Metal Dichalcogenide Monolayers*, *Phys. Rev. B* **93**, 121107 (2016).
- [65] D. Y. Qiu, T. Cao, and S. G. Louie, *Nonanalyticity, Valley Quantum Phases, and Lightlike Exciton Dispersion in Monolayer Transition Metal Dichalcogenides: Theory and First-Principles Calculations*, *Phys. Rev. Lett.* **115**, 176801 (2015).
- [66] Z. Wang, L. Zhao, K. F. Mak, and J. Shan, *Probing the Spin-Polarized Electronic Band Structure in Monolayer Transition Metal Dichalcogenides by Optical Spectroscopy*, *Nano Lett.* **17**, 740 (2017).
- [67] X. Zhang, T. Cao, Z. Lu, Y. Lin, F. Zhan, Y. Wang, Z. Li, J. C. Hone, J. A. Robinson, D. Smirnov, S. G. Louie, and T. F. Heinz, *Magnetic Brightening and Control of Dark Excitons in Monolayer WSe₂*, [arXiv:1612.03558](https://arxiv.org/abs/1612.03558).
- [68] M. R. Molas, C. Faugeras, A. O. Slobodeniuk, K. Nogajewski, M. Bartos, D. M. Basko, and M. Potemski, *Brightening of Dark Excitons in Monolayers of Semiconducting Transition Metal Dichalcogenides*, *2D Mater.* **4**, 021003 (2017).
- [69] K. P. O'Donnell and X. Chen, *Temperature Dependence of Semiconductor Bandgaps*, *Appl. Phys. Lett.* **58**, 2924 (1991).
- [70] J. W. Christopher, B. B. Goldberg, and A. K. Swan, *Long Tailed Trions in Monolayer MoS₂: Temperature Dependent Asymmetry and Red-Shift of Trion Photoluminescence Spectra*, [arXiv:1605.09741](https://arxiv.org/abs/1605.09741).
- [71] G. Kioseoglou, A. Hanbicki, M. Currie, A. L. Friedman, and B. T. Jonker, *Optical Polarization and Intervalley Scattering in Single Layers of MoS₂ and MoSe₂*, *Sci. Rep.* **6**, 25041 (2016).
- [72] M. Selig, G. Berghauser, A. Raja, P. Nagler, C. Schuller, T. F. Heinz, T. Korn, A. Chernikov, E. Malic, and A. Knorr, *Excitonic Linewidth and Coherence Lifetime in Monolayer Transition Metal Dichalcogenides*, *Nat. Commun.* **7**, 13279 (2016).
- [73] G. Moody, C. K. Dass, K. Hao, C. H. Chen, L. Li, A. Singh, K. Tran, G. Clark, X. Xu, G. Berghauser, E. Malic, A. Knorr, and X. Li, *Intrinsic Homogeneous Linewidth and Broadening Mechanisms of Excitons in Monolayer Transition Metal Dichalcogenides*, *Nat. Commun.* **6**, 8315 (2015).
- [74] C. Klingshirn, *Semiconductor Optics*, 3rd ed. (Springer, Berlin, 2007).
- [75] This makes an exact determination of the Stokes shift between reflectivity and PL difficult, as the laser and white light spots need to overlap perfectly and have the same diameter. This is of course roughly the case in our experiment, and we estimate an upper limit of the Stokes shift of 5 meV, not excluding that it is close to zero for certain positions on the sample.
- [76] D. Xiao, G.-B. Liu, W. Feng, X. Xu, and W. Yao, *Coupled Spin and Valley Physics in Monolayers of MoS₂ and Other Group-VI Dichalcogenides*, *Phys. Rev. Lett.* **108**, 196802 (2012).
- [77] K. F. Mak, K. He, J. Shan, and T. F. Heinz, *Control of Valley Polarization in Monolayer MoS₂ by Optical Helicity*, *Nat. Nanotechnol.* **7**, 494 (2012).
- [78] G. Sallen, L. Bouet, X. Marie, G. Wang, C. R. Zhu, W. P. Han, Y. Lu, P. H. Tan, T. Amand, B. L. Liu, and B. Urbaszek, *Robust Optical Emission Polarization in MoS₂ Monolayers through Selective Valley Excitation*, *Phys. Rev. B* **86**, 081301 (2012).
- [79] K. Hao, G. Moody, F. Wu, C. K. Dass, L. Xu, C.-H. Chen, M.-Y. Li, L.-J. Li, A. H. MacDonald, and Xiaoqin Li, *Direct Measurement of Exciton Valley Coherence in Monolayer WSe₂*, *Nat. Phys.* **12**, 677 (2016).
- [80] F. Meier and B. Zakharchenya, *Optical Orientation*, Modern Problems in Condensed Matter Sciences Vol. 8 (North-Holland, Amsterdam, 1984).
- [81] M. Z. Maialle, E. A. de Andrade e Silva, and L. J. Sham, *Exciton Spin Dynamics in Quantum Wells*, *Phys. Rev. B* **47**, 15776 (1993).
- [82] M. M. Glazov, E. L. Ivchenko, G. Wang, T. Amand, X. Marie, and B. Urbaszek, *Spin and Valley Dynamics of Excitons in Transition Metal Dichalcogenide Monolayers*, *Phys. Status Solidi B* **252**, 2349 (2015).
- [83] P. Le Jeune, X. Marie, T. Amand, F. Romstad, F. Perez, J. Barrau, and M. Brousseau, *Spin-Dependent Exciton-Exciton Interactions in Quantum Wells*, *Phys. Rev. B* **58**, 4853 (1998).
- [84] E. L. Ivchenko, *Spin Physics in Semiconductor Nanostructures* (Harrow, Alpha Science, Oxford, England, 2005).
- [85] D. K. Efimkin and A. H. MacDonald, *Many-Body Theory of Trion Absorption Features in Two-Dimensional Semiconductors*, *Phys. Rev. B* **95**, 035417 (2017).
- [86] P. Back, M. Sidler, O. Cotlet, A. Srivastava, N. Takemura, M. Kroner, and A. Imamoglu, *Giant Paramagnetism*

- Induced Valley Polarization of Electrons in Charge-Tunable Monolayer MoSe₂, arXiv:1701.01964.*
- [87] D. Press, T. D. Ladd, B. Zhang, and Y. Yamamoto, *Complete Quantum Control of a Single Quantum Dot Spin Using Ultrafast Optical Pulses*, *Nature (London)* **456**, 218 (2008).
- [88] S. Dufferwiel, T. P. Lyons, D. D. Solnyshkov, A. A. P. Trichet, F. Withers, S. Schwarz, G. Malpuech, J. M. Smith, K. S. Novoselov, M. S. Skolnick, D. N. Krizhanovskii, and A. I. Tartakovskii, *Valley Addressable Exciton-Polaritons in Atomically Thin Semiconductors*, arXiv:1612.05073.
- [89] Y.-J. Chen, J. D. Cain, T. K. Stanev, V. P. Dravid, and N. P. Stern, *Valley-Polarized Exciton-Polaritons in a Monolayer Semiconductor*, arXiv:1701.05579.
- [90] C. Mai, A. Barrette, Y. Yu, Y. G. Semenov, K. W. Kim, L. Cao, and K. Gundogdu, *Many-Body Effects in Valleytronics: Direct Measurement of Valley Lifetimes in Single-Layer MoS₂, Nano Lett.* **14**, 202 (2014).
- [91] L. Yang, N. A. Sinitsyn, W. Chen, J. Yuan, J. Zhang, J. Lou, and S. A. Crooker, *Long-Lived Nanosecond Spin Relaxation and Spin Coherence of Electrons in Monolayer MoS₂ and WS₂, Nat. Phys.* **11**, 830 (2015).
- [92] O. A. Ajayi, J. V. Ardelean, G. D. Shepard, J. Wang, A. Antony, T. Taniguchi, K. Watanabe, T. F. Heinz, S. Strauf, X.-Y. Zhu, and J. C. Hone, *Approaching the Intrinsic Photoluminescence Linewidth in Transition Metal Dichalcogenide Monolayers*, arXiv:1702.05857.
- [93] A. Castellanos-Gomez, M. Buscema, R. Molenaar, V. Singh, L. Janssen, H. S. J. van der Zant, and G. A. Steele, *Deterministic Transfer of Two-Dimensional Materials by All-Dry Viscoelastic Stamping*, *2D Mater.* **1**, 011002 (2014).